Flow-cytometric light scattering measurement of red blood cell volume and hemoglobin concentration

D. H. Tycko, M. H. Metz, E. A. Epstein, and A. Grinbaum

A light scattering technique for simultaneously determining the volume (V) and hemoglobin concentration (HC) of individual sphered red blood cells (RBCs) is described. Light scattered into two angular intervals yields measurements S_1 and S_2, respectively. Since a sphered RBC is essentially a homogeneous dielectric sphere having a complex refractive index that is linear in HC, with a proper choice of detector acceptance angles, tables relating V and HC to S_1 and S_2 can be computed via Mie theory. Absolute calibration is possible using droplets of water-immisible oils of accurately known refractive index. Results of experimental tests of the method are compared with those obtained from hematological reference measurements.

I. Introduction

The use of forward light scattering to estimate the relative size of individual biological cells is a well-established technique in flow cytometry.[1] In general, the angular distribution of the light scattered by a particle depends not only on the volume of the particle but also on its shape, orientation, and refractive-index distribution.[2] These factors complicate the interpretation of light scattering data, limiting the accuracy and precision of absolute size measurements. In clinical hematology, however, there is a need for accurate and precise measurements of the volume of individual red blood cells.

The red blood cells in a patient sample are characterized by the mean cell volume (MCV), the mean cell hemoglobin concentration (MCHC), the mean cell hemoglobin mass (MCH),[3] and the red cell volume distribution width expressed as a coefficient of variation (RDW).[4] Several clinical laboratory instruments for measuring these red cell indices employ flow-cytometric methods to measure the cell volume distributions from which MCV and RDW are derived. The Technicon H6000 system (Technicon Instruments Corp., Tarrytown, N.Y.) and the Ortho ELT-8 system (Ortho Diagnostic Systems, Inc., Westwood, Mass.) both use forward light scattering at one angular interval to measure the red cell volume distribution. The Coulter S series of instruments (Coulter Electronics, Inc., Hialeah, Fla.) uses electronic resistive pulse sizing.[5] For all these instruments, the accuracy of individual cell volume measurements is limited by factors which depend on the unknown hemoglobin concentration within each cell, a quantity which varies from one cell to the next in a blood sample.[6,7] In the case of the light scattering systems, the hemoglobin concentration within a cell determines the refractive index of the cell and, consequently, the amount of light scattered into the angular interval accepted by the detection optics. Therefore, there is an uncertainty in the volume to be associated with a given scatter signal. A similar source of error exists in electrical sizing instruments. The resistive pulse measured in these devices depends on the deformation of the cell as it passes through the sensing orifice and this deformation is determined by the cell fluid viscosity which is highly dependent on the unknown and variable hemoglobin concentration.

The method to be described in this paper overcomes the problem of hemoglobin concentration interference in red blood cell volume measurements. This is done by simultaneously determining both the volume and the hemoglobin concentration of each cell. Scattered monochromatic light at two different forward angular intervals is measured. The shape and orientation dependence of the scattering is eliminated by isovolumetrically sphering the cells using the method of Kim and Ornstein.[8] The sphered cells are essentially homogeneous dielectric spheres. Mie scattering theory[9] accurately describes the scattering by these sphered cells. Therefore, with a proper choice of angular intervals, a one-to-one mapping between the two scattering signals

When this work was done all authors were with Technicon Instruments Corporation, 511 Benedict Avenue, Tarrytown, New York 10591; E. A. Epstein is now with the IBM Thomas J. Watson Research Laboratories, Yorktown Heights, New York 10598.

Received 19 October 1984.
0003-6935/85/091355-11$02.00/0.

and pairs of volume and hemoglobin concentration values can be constructed. With such a mapping available, the method allows accurate and precise measurements of the volume and hemoglobin concentration for each cell in a blood sample. A 2-D frequency distribution of volume vs hemoglobin concentration can be constructed from these measurements. The statistics of this frequency distribution include the MCV, MCHC, and RDW of the sample and two additional parameters which give the hemoglobin concentration distribution width (HDW) and the correlation between the two measurements, respectively.

The theoretical basis of the method is presented in detail in Secs. II and III. The equipment and procedures used to test the method are described in Sec. IV. Experimental results are given in Sec. V. Absolute optical calibration of hematology instruments has been a difficult problem. This question is addressed in Sec. VI where an absolute optical calibration procedure is described.

II. Optical Model of a Red Blood Cell

A normal human red blood cell (RBC) has a biconcave discoid shape which complicates the interpretation of light scattering data. However, Kim and Ornstein[8] have developed a procedure for isovolumetrically sphering red cells prior to flow-cytometric analysis. Their sample preparation method is assumed here and was used in the experiments described below.

Generally, a biological cell consists of a surrounding membrane containing a nucleus and other organelles in a cytoplasmic solution of proteins and electrolytes. The refractive-index distribution of such a system is not simple and varies from one cell to another. However, a mature RBC does not contain a nucleus or any other cytoplasmic organelles. This internal homogeneity is seen clearly in transmission electron micrographs of the sphered RBCs.[8]

The optical properties of the red cell membrane are primarily determined by a lipid bilayer having a thickness[10] of ~7 nm and a refractive index[11] near 1.46. A typical sphered RBC has a diameter of 5.5 μm and a cytoplasmic refractive index of 1.40. Using the Rayleigh-Gans approximation,[12] the contribution of the membrane to the relevant forward light scattering cross sections was estimated to be <1% in the typical case and <2% in the atypical worst case of a small RBC with low hemoglobin concentration.

Consequently, from the point of view of optical properties, a RBC will be modeled as a homogeneous aqueous solution of hemoglobin (~34 g/dliter), salts (~0.7 g/dliter), and other organic compounds (~0.2 g/dliter)[13] contained in a transparent cell membrane of negligible thickness. The water and hemoglobin molecules occupy more than 95% of the cell volume.[10] Therefore, with respect to forward light scattering, a sphered RBC can be characterized by a volume V and a complex index of refraction $n_c = n_R - in_I$. Since the interior of the cell is almost completely occupied by water and hemoglobin, variations in n_c from cell to cell can be attributed solely to variations in hemoglobin concentration, HC. The real part of n_c is related to HC by[11]

$$n_R = n_0 + \alpha \cdot \mathrm{HC}, \tag{1}$$

where α is the specific refraction increment of hemoglobin and n_0 is the refractive index of the cell fluid in the absence of hemoglobin. The radiation wavelength interval of interest in this investigation is between 0.5 and 1.2 μm; in this range α and n_0 have typical values of 0.0019 dliter/g and 1.34, respectively. In this same range, hemoglobin is the only cell constituent exhibiting a significant amount of absorption. Consequently, assuming Beer's law applies,[14] the imaginary part of n_c is given by

$$n_I = \frac{\ln 10}{\pi M} \lambda \epsilon_{\mu M} \cdot \mathrm{HC}, \tag{2}$$

where M is the molecular weight of hemoglobin (66,500), λ is the wavelength in micrometers, and $\epsilon_{\mu M}$ is the micromolar extinction coefficient of hemoglobin at wavelength λ in cm^2/micromole.[15] Thus, for a given wavelength, the complex index of refraction of a RBC is determined through Eqs. (1) and (2) by a single physical variable, the cell hemoglobin concentration.

III. Theory of the Method

For the above model of a sphered RBC, Mie scattering theory applies. We shall be interested in the differential cross section $d\sigma/d\theta$ for scattering into a conical shell of half-angle θ centered on the incident beam direction. For a plane polarized incident wave

$$\frac{d\sigma}{d\theta} = \frac{\sin\theta}{k^2} \int_0^{2\pi} (i_1 \sin^2\phi + i_2 \cos^2\phi) d\phi = \frac{\pi}{k^2} (i_1 + i_2) \sin\theta, \tag{3}$$

where $k = 2\pi n_s/\lambda$ and n_s is the refractive index of the nonabsorbing medium in which the cells flow. The scattering intensity functions i_1 and i_2 are those defined by Kerker.[9] The former refers to scattered radiation polarized perpendicular to the scattering plane, the latter to scattered radiation polarized parallel to the scattering plane. They are functions of V, HC, λ, n_s, and θ. The angular dependence of $d\sigma/d\theta$ is displayed in Fig. 1 for $\lambda = 0.842$ μm and values of V and HC covering the typical RBC range. It is apparent that information on both V and HC is contained in these forward scattering angular distributions. We have found that this information can be extracted by sampling at two appropriately chosen angular intervals and that accurate and precise simultaneous measurements of V and HC are obtainable.

A conventional dark-field electrooptical system for measuring the light scattered into an angular interval in the forward direction is shown schematically in Fig. 2(A). A monochromatic collimated light beam illuminates a sphered RBC in the sample stream of a sheathed-stream flow cell. A dark stop with an annular clear region blocks the incident beam and passes light scattered between angles θ and $\theta + \Delta\theta$. The scattered light is focused on a photodetector whose output is amplified by a factor G. As a RBC passes through the illuminating beam, a pulse having peak height S is

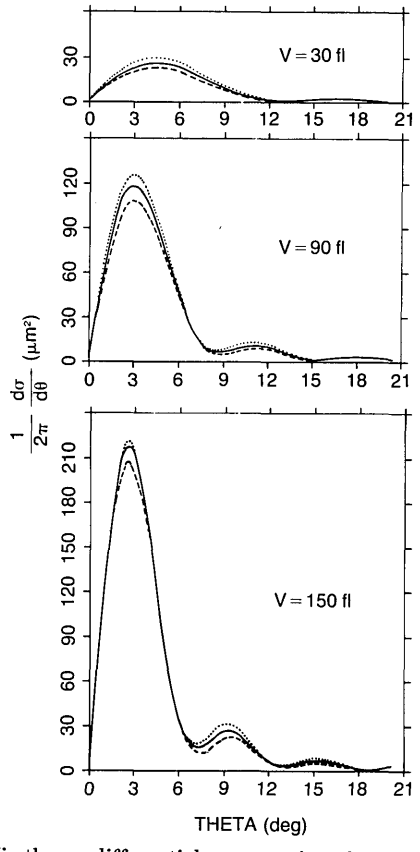

Fig. 1. Mie theory differential cross sections for scattering into a conical shell of half-angle θ about the incident beam direction. Dashed curves, HC = 31 g/dliter; solid curve, HC = 34 g/dliter; dotted curves, HC = 37 g/dliter. $\lambda = 0.842\ \mu m$, $n_s = 1.330$, $n_0 = 1.335$, $\alpha = 0.001942$ dliter/g, $\epsilon_{\mu M} = 0.2520\ cm^2/\mu M$.

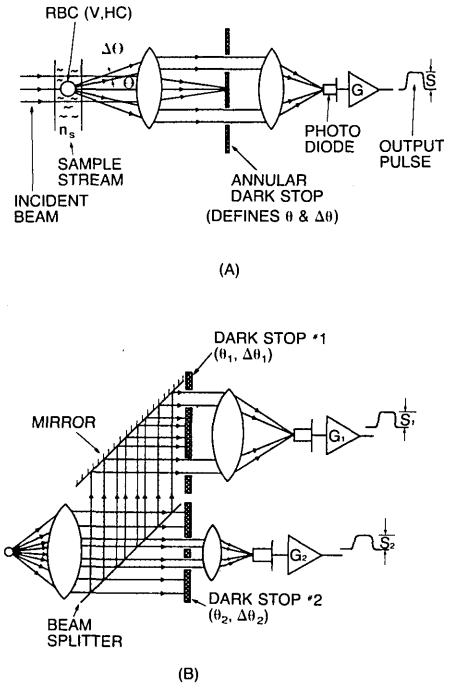

Fig. 2. Schematic diagrams of dark-field systems for measuring the light scattered by a sphered red blood cell characterized by volume V and hemoglobin concentration HC, flowing in a fluid having refractive index n_s. (A) Single-angular interval detection; (B) double-angular interval detection.

produced at the amplifier output. This pulse height is a function of the known system parameters λ, n_s, θ, $\Delta\theta$, G and the unknown quantities V and HC. The gain factor G may be chosen to make S equal the cross section for scattering into the angular interval between θ and $\theta + \Delta\theta$, in which case

$$S = \int_{\theta}^{\theta+\Delta\theta} (d\sigma/d\theta')d\theta' = f(\lambda,n_s,\theta,\Delta\theta;V,\mathrm{HC}). \quad (4)$$

By numerical integration of angular distributions such as those in Fig. 1, the response of S to variations in V and HC can be computed. Figure 3(B) illustrates the response curves obtained for a radiation wavelength of 0.842 μm and an angular interval between 3° and 5.5°. The dependence of S on V and HC seen in Fig. 3(B) is characteristic of systems in which the accepted angular interval of the scattered light lies below the first minimum of the angular distribution for all values of V and HC in their expected ranges. Clearly, a measurement of S does not uniquely determine the V and HC values of the RBC producing the scattered light. This indeterminacy reflects the fact that we are dealing with a single equation, Eq. (4), in two unknowns, V and HC.

To remove the indeterminacy, at least two values of S, corresponding to two different sets of system parameters, must be measured for each RBC. This may be done without complicating the illumination optics by measuring the light scattered into two different angular intervals. Figure 2(B) represents a system for doing this in which an optical channel accepting scattered light in the angular interval between θ_1 and $\theta + \Delta\theta_1$ produces a signal S_1 while a signal S_2 is produced in a channel with a different acceptance interval, θ_2 to $\theta_2 + \Delta\theta_2$. The behavior of this type of system is described by two response equations:

$$S_1 = \int_{\theta_1}^{\theta_1+\Delta\theta_1} (d\sigma/d\theta')d\theta' = f(\lambda,n_s,\theta_1,\Delta\theta_1;V,\mathrm{HC}), \quad (5a)$$

$$S_2 = \int_{\theta_2}^{\theta_2+\Delta\theta_2} (d\sigma/d\theta')d\theta' = f(\lambda,n_s,\theta_2,\Delta\theta_2;V,\mathrm{HC}), \quad (5b)$$

thus yielding two equations in the two unknowns V and HC.

Equations (5a) and (5b) will yield unique solutions for V and HC in the region of the (V,HC) domain where their Jacobian determinant is nonzero. That is,

$$J = \left|\frac{\partial S_1}{\partial V}\frac{\partial S_2}{\partial \mathrm{HC}} - \frac{\partial S_1}{\partial \mathrm{HC}}\frac{\partial S_2}{\partial V}\right| \neq 0. \quad (6)$$

Whether this solvability condition is satisfied depends sensitively on the angular intervals chosen. A solvable system may be defined as a set of system parameters $\{\lambda,n_s,\theta_1,\Delta\theta_1,\theta_2,\Delta\theta_2\}$ for which Eq. (6) is satisfied whenever V and HC are within the required ranges. For red blood cells, such ranges typically would be 30 fliter to 150 fliter for V and 22 g/dliter to 46 g/dliter for HC. The elements of the Jacobian determinant can be calculated from the pair of response curves corresponding to the chosen pair of angular intervals. Figure 3 dis-

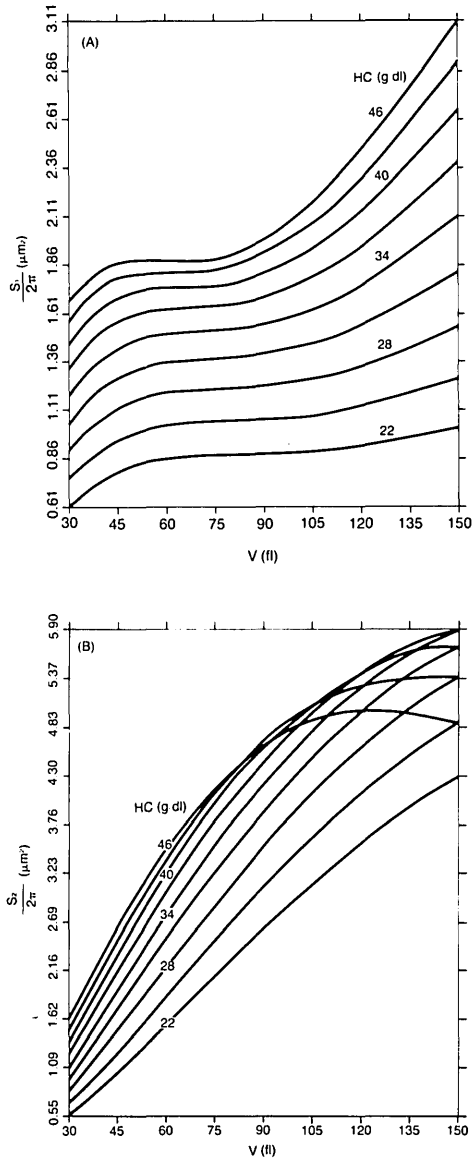

Fig. 3. Cross sections for scattering into finite angular intervals as functions of V and HC. Wavelength and refractive-index parameters as given in Fig. 1. (A) S_1 is the cross section for $\theta = 5.5°$, $\Delta\theta = 5.0°$. (B) S_2 is the cross section for $\theta = 3.0°$, $\Delta\theta = 2.5°$.

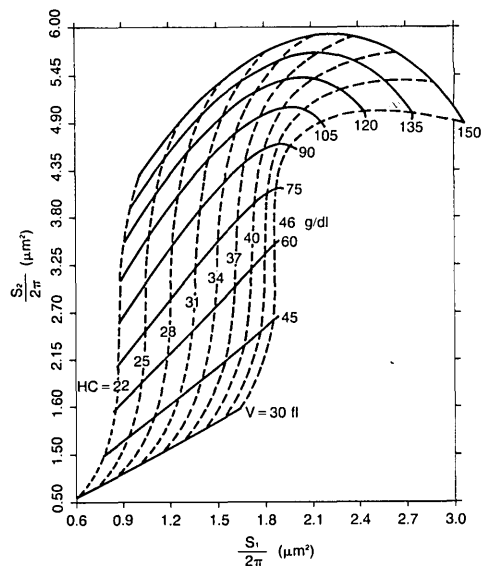

Fig. 4. Mapping of (S_1,S_2) pairs into (V,HC) pairs for a solvable system. Solid curves are constant-V contours; dashed curves are constant-HC contours. System parameters are those of Figs. 1 and 3.

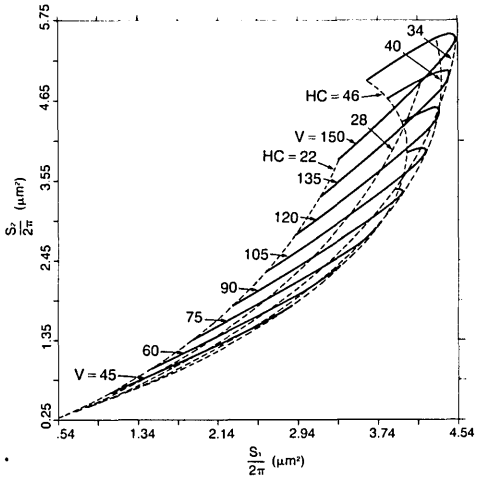

Fig. 5. The (S_1,S_2) to (V,HC) mapping for an unsolvable system. Wavelength and refractive index parameters as given in Fig. 1. $\theta_1 = 3.5°$, $\Delta\theta_1 = 2.5°$, $\theta_2 = 2.0°$, $\Delta\theta_2 = 1.5°$.

plays the two response curves for a solvable system with $\lambda = 0.842\ \mu$m, a low-angle interval between 3° and 5.5°, and a higher-angle interval between 5.5° and 10.5°. The solvability of this system is most easily seen by considering Fig. 4 where for each (V,HC) pair, the corresponding (S_1,S_2) pair is plotted. The solvability is apparent since the constant-V curves are well separated from one another and the constant-HC curves are also well separated from one another. To characterize solvability generally, consider any two (V,HC) pairs which differ by the resolution requirements of the system. Then the system is solvable if the corresponding two (S_1,S_2) points are separated by a practicably measurable amount and if each (S_1,S_2) point corresponds to a unique (V,HC) pair. This one-to-one correspondence between (S_1,S_2) and (V,HC) pairs makes it possible to construct tables of V and HC vs (S_1,S_2) pairs which can be stored in the memory of the computer used to process the measurements.

For comparison, the (S_1,S_2) plot for an unsolvable system is given in Fig. 5. Since there is poor separation and crossing of HC contours as well as crossing of V contours, tables mapping (S_1,S_2) pairs into (V,HC) pairs cannot be constructed for this choice of angular intervals.

IV. Experimental Equipment and Procedures

The optical system shown in Fig. 6 was used to test the method described above. The light source was a GaAlAs diode laser integrated with a Selfoc microlens (M/A-COM Laser Diode Laboratories LCW-30) which produces a 1-mm diam circular beam with a 10-mrad divergence and a wavelength of 0.842 μm. The beam, focused in one direction by a 100-mm cylindrical lens

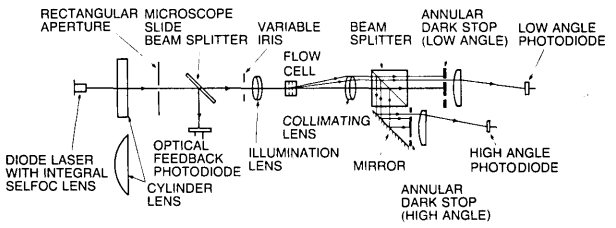

Fig. 6. Schematic diagram of the experimental optical system.

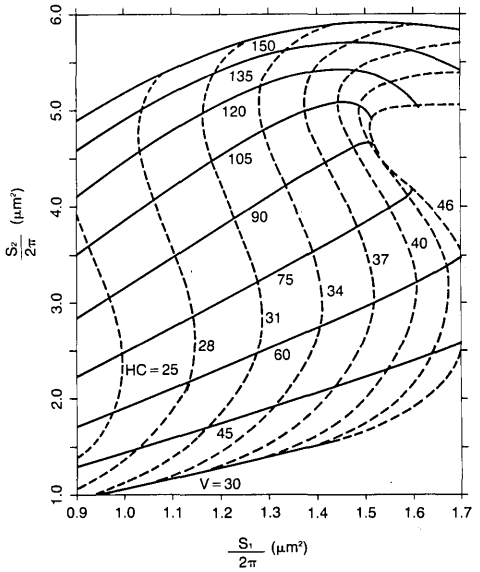

Fig. 7. The (S_1,S_2) to (V,HC) mapping for the experimental system of Fig. 6. Wavelength and refractive-index parameters as given in Fig. 1. $\theta_1 = 5.5°$, $\Delta\theta_1 = 3.5°$, $\theta_2 = 3.0°$, $\Delta\theta_2 = 2.5°$. Only that region of the S_1-S_2 plane used in the data analysis is shown.

(Rolyn 14.0250), illuminated a 100- × 400-μm rectangular aperture. The rectangular aperture was imaged with ~4:1 demagnification in the center of the viewing volume of the sheathed-stream flow cell by a 50-mm doublet lens (Melles-Griot 01-LAU-022). The radiant power in the flow cell was 370 μW when the diode laser output was 2.8 mW. A small amount of light was split from the beam just after the rectangular aperture and monitored by a photodiode for the purpose of beam power normalization.

The light scattered by a RBC in the sample stream was collected and collimated by a 40-mm doublet lens (Melles-Griot 01-LA0-037) and divided by a cube beam splitter into two optical channels, designated high angle and low angle, respectively. Using a ray tracing analysis of the optical system, the radii of the annular dark stops were set for an angular interval of 3.0–5.5° (i.e., $\theta_2 = 3.0°$, $\Delta\theta_2 = 2.5°$) in the low-angle channel and 5.5–9.0° (i.e., $\theta_1 = 5.5°$, $\Delta\theta_1 = 3.5°$) in the high-angle channel. The 150-mm detector lenses (Rolyn 10.0330) behind the dark stops imaged the central plane of the flow cell viewing volume on the photodiode detectors. The detectors had sensitive areas of 5 mm² (Centronic OSD5-OA).

The numerical aperture of the available collection lens was not large enough to accept the 10.5° high-angle

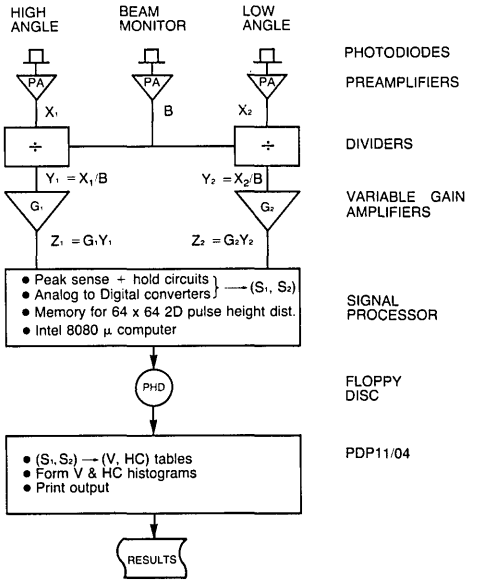

Fig. 8. Block diagram of the experimental data acquisition and analysis system.

interval upper limit ($\Delta\theta_1 = 5.0°$) of the solvable system discussed above. The effect of this restriction can be seen by comparing Fig. 4 with Fig. 7, the S_1–S_2 plot for the experimental optical system. The compression of the constant HC curves for HC above 40 g/dliter and V between 75 fliter and 105 fliter causes a loss of resolution in HC in a small region of the S_1-S_2 plane. However, the system is still solvable.

The sheathed-stream flow cell was the type used in the Technicon Hemalog D and H6000 instruments.[16] Fluids were driven by standard H6000 peristaltic pumps. Flow rates and tubing diameters were chosen to give a sample stream diameter of 35 μm. The sphered red cells in the sample stream had a velocity of ~1 m/sec. The sample fluid consisted of ~1 μliter of a whole blood sample mixed with 5 mliter of the Kim-Ornstein RBC sphering reagent. Immediately after mixing, the sample was aspirated. Signal processing began 50 sec after the whole blood was dropped into the reagent. A 10-sec data acquisition period produced between 2000 and 10,000 cell measurements per sample.

A block diagram of the data acquisition and analysis systems is given in Fig. 8. The photodetector scatter signals were normalized to the radiant power in the flow cell and the two normalized pulses were amplified by gain factors G_1 and G_2, respectively. The peaks of the two pulses were then sensed and digitized, forming the two measurements S_1 and S_2. A 64 × 64 2-D pulse height distribution was accumulated for each sample and recorded on a floppy disk for later analysis on a PDP 11/04 computer. The PDP 11 analysis program contains the precomputed tables of V and HC values vs pairs of S_1 and S_2 values. Using these tables, V and HC histograms were constructed from the pulse height distribution. The means, MCV and MCHC, and standard deviations, σ_V and σ_{HC}, of the two histograms were computed. The gain factors G_1 and G_2 were set

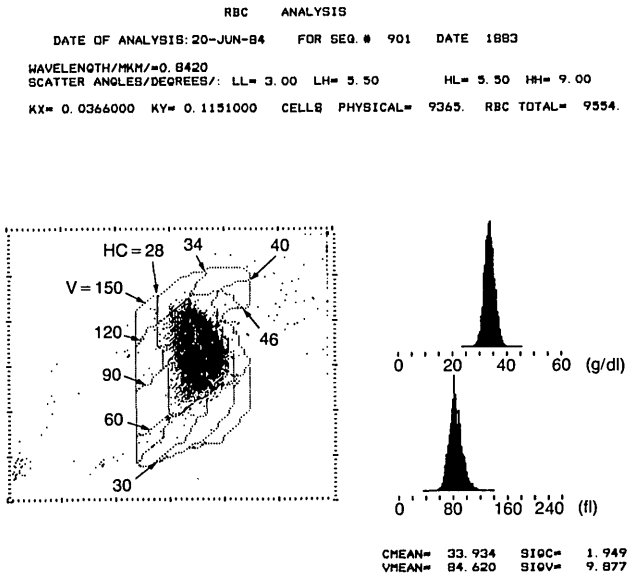

Fig. 9. Example of the output produced by the PDP 11 data analysis program. The abscissa (X) and ordinate (Y) axes of the 2-D pulse height distribution (cytogram) on the left have units of channel number (0–60). The top histogram on the right gives the HC distribution, the bottom histogram gives the V distribution. Means and standard deviations of these distributions are printed below the histograms. System parameters and cell counts are listed at the top. K_x and K_y are conversion factors between pulse height channel numbers and cross sections in μm^2 ($S_1 = 2\pi K_x X$, $S_2 = 2\pi K_y Y$). Physical cells, the number of events falling within the (V,HC) grid; RBC total cells, the total event count.

to yield S_1 and S_2 values having the same units as those used in the precomputed $(S_1,S_2) \rightarrow (V,HC)$ mapping tables. The calibration procedure for doing this is described below.

In addition to the two histograms and their statistics, the output listing, Fig. 9, contains a grey-scale representation of the 2-D pulse height distribution. Such a two-parameter display is called a cytogram. A grid of V and HC contours is superimposed on the cytogram for the purpose of semiquantitative visual interpretation of the (S_1,S_2) distributions in terms of V and HC. Data falling outside the boundaries of this grid are not included in the analysis and, therefore, do not contribute to the V and HC histograms.

The purpose of the experiments was to test the method by comparing the measured values of MCV and MCHC to values determined by an accepted reference method. Reference values for MCV were calculated from carefully measured hematocrits (defined as the percent of the whole blood volume occupied by red cells) and red cell counts (defined as the number of red cells per microliter of whole blood). Reference MCHC values were derived from the hematocrits and the whole blood hemoglobin concentrations. Hematocrits were measured by spinning microhematocrit tubes for 10 min at 11,500 rpm in a microhematocrit centrifuge.[17] The tubes were measured using a microscope stage micrometer at 50× magnification. The red cell counts were measured electronically using a Coulter ZBI cell counter. Whole blood hemoglobin concentrations were measured spectrophotometrically using the hemiglobincyanide method.[18]

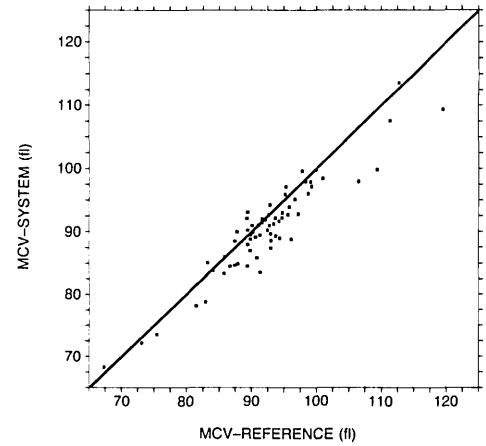

Fig. 10. Comparison of MCV measurements from the experimental system with reference values for randomly selected hospital samples. Solid line represents identity. Linear regression results ($y = ax + b$): number of samples $N = 72$; mean $MCV_{REF} = 92.4$; s.d. $MCV_{REF} = 7.3$; mean $MCV_{SYS} = 90.4$; s.d. $MCV_{SYS} = 7.3$; slope $a = 0.87$; intercept $b = 10.10$; s.d. of regression $Syx = 2.50$; correlation coefficient $r = 0.94$.

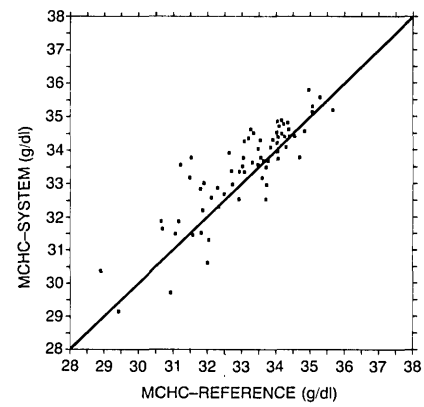

Fig. 11. Comparison of MCHC measurements from the experimental system with reference values for randomly selected hospital samples. $N = 72$; mean $MCHC_{REF} = 33.1$; s.d. $MCHC_{REF} = 1.4$; mean $MCHC_{SYS} = 33.4$; s.d. $MCHC_{SYS} = 1.4$; $a = 0.85$; $b = 5.30$; $Syx = 0.68$; $r = 0.87$.

Calibration of the system was done using ten normal whole blood samples. The gains G_1 and G_2 were adjusted until the averages of the ten measured MCV and MCHC values agreed exactly with the averages of the corresponding ten reference values.

V. Experimental Results

In the first experiment, seventy-two randomly selected blood samples were obtained from Westchester County Medical Center. For each blood sample, MCV and MCHC were measured on the experimental system and the values compared with the reference values. As can be seen in the correlation plots of Figs. 10 and 11, there was generally close agreement between the system measurements and the reference values. One source of the differences between the system and reference

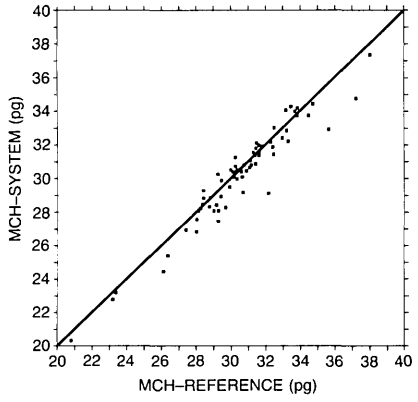

Fig. 12. Comparison of MCH values from the experimental system with reference values for randomly selected hospital samples ($MCH_{SYS} = MCV_{SYS} \cdot MCHC_{SYS}/100$). $N = 72$; mean $MCH_{REF} = 30.6$; s.d. $MCH_{REF} = 2.8$; mean $MCH_{SYS} = 30.3$; s.d. $MCH_{SYS} = 2.9$; $a = 0.98$; $b = 2.5$; $Syx = 0.80$; $r = 0.96$.

values is an osmotic effect. The system values were measured with red cells suspended in the sphering reagent which had a constant osmolality. The reference values were for cells suspended in their native plasma, a medium with a composition and osmolality which varies from sample to sample. Each red cell adapts to these small osmolality changes by exchanging water with its environment, causing small changes in V and HC. Another source of the differences is the positive error in hematocrit caused by the trapping of plasma between the packed red cells during the centrifugation of the microhematocrit tubes. This error is between 1% and 3% for normal samples and can be as high as 6% in certain types of abnormal samples.[17] (Samples containing sickled cells, which can cause even larger trapped-plasma errors, were not included in our data.) These errors propagate directly as positive errors in reference MCV values and negative errors in reference MCHC values.

Since the mass of hemoglobin within a cell is not affected by the exchange of water, the product of V and HC should be independent of osmolality. Furthermore, the trapped-plasma error in the hematocrit does not affect the reference MCH value which is calculated by dividing the whole blood hemoglobin concentration by the red cell count. Therefore, a reference MCH value was calculated for each sample and compared with the system value computed as the product of (MCV/10) and (MCHC/10). The results are plotted in Fig. 12. Elimination of the osmotic and trapped-plasma effects clearly improves the agreement between reference and system measurements.

In the second experiment, aliquots of two blood samples were subjected to a procedure in which the red cells were hydrated (swollen) or dehydrated (shrunken) and left in an isotonic phosphate-buffered saline solution.[19] This procedure can produce samples with MCV and MCHC values covering a relatively wide range without any variability in osmolality. Furthermore, they can be handled in exactly the same way as natural whole blood samples. The comparison of system

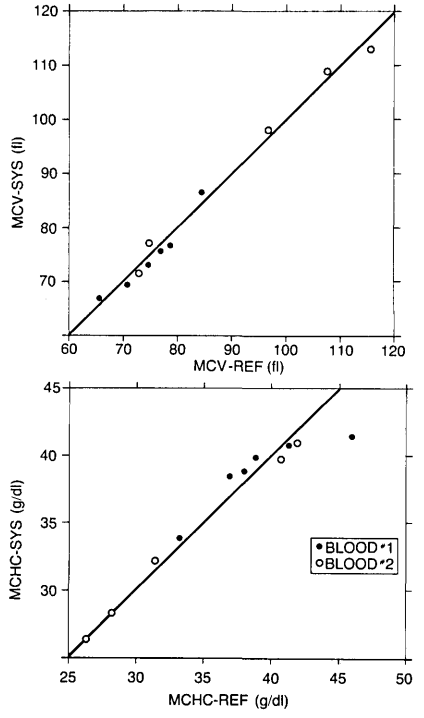

Fig. 13. Comparisons of system measurements of MCV and MCHC with reference values for samples consisting of red cells in altered hydration states. MCV results (top): $N = 11$, mean $MCV_{REF} = 83.6$; s.d. $MCV_{REF} = 16.2$; mean $MCV_{SYS} = 83.5$; s.d. $MCV_{SYS} = 16.2$; $a = 1.00$; $b = 0.26$; $Syx = 1.67$, $r = 0.99$. MCHC results (bottom): $N = 10$ (outlier excluded); mean $MCHC_{REF} = 35.7$; s.d. $MCHC_{REF} = 5.6$; mean $MCHC_{SYS} = 36.0$; s.d. $MCHC_{REF} = 5.4$; $a = 0.96$; $b = 1.71$; $Syx = 0.82$; $r = 0.99$.

measurements with reference values (Fig. 13) for eleven samples prepared in this manner shows close agreement over somewhat extended ranges of MCV and MCHC. The outlier in the MCHC data was due to the arbitrary cutoff at HC = 46 g/dliter in the $(S_1,S_2) \rightarrow (V,HC)$ tables which excluded cells having higher HC values from the histograms.

The next experiment was designed to test the sensitivity of the method to variations in the HC distribution of a blood sample. The density of a red cell is linearly dependent on its hemoglobin concentration. Consequently, a whole blood sample may be separated into fractions having successively higher values of MCHC by centrifuging on a discontinuous Stractan density gradient.[20,21] The fractions are extracted from the regions of the Stractan column between adjacent density layers. Five fractions of a normal sample were prepared using this technique. A reference MCHC was determined for each fraction. As can be seen in Table I, there is precise agreement of these reference values with the MCHC measurements made on the experimental system. The table also contains the results of the σ_{HC}, MCV, and σ_V measurements for each fraction. To illustrate the systematic changes in the data associated with the density progression, the cytograms and histograms obtained from the top, middle, and bottom density fractions are shown in Fig. 14. Four more samples, each having a uniquely different cellular

Table I. System Measurement Results for Five Fractions of a Normal Blood Sample Separated on a Discontinuous Stractan Density Gradient; for Comparison, the Reference MCHC Values for Each Fraction are Also Tabulated

Fraction	$MCHC_{REF}$ (g/dliter)	$MCHC_{SYS}$ (g/dliter)	σ_{HC} (g/dliter)	MCV_{SYS} (fliter)	σ_V (fliter)
1	29.9	30.6	1.6	93.9	12.2
2	32.1	32.0	1.4	89.2	10.5
3	34.0	34.0	1.9	84.8	10.3
4	37.5	37.5	2.1	77.2	9.9
5	39.7	39.3	2.6	72.2	10.3

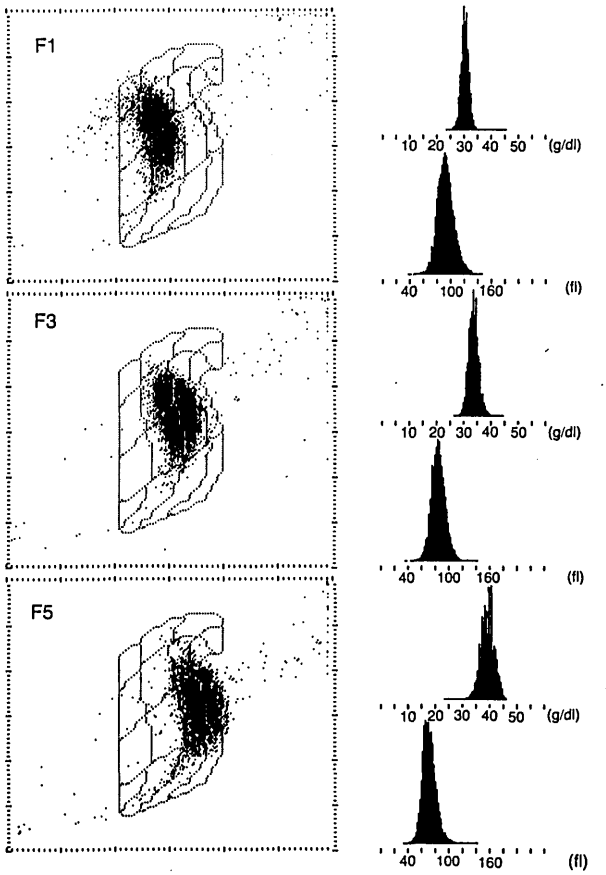

Fig. 14. Cytograms and histograms associated with the top ($F1$), middle ($F3$), and bottom ($F5$) fractions of a whole blood sample separated into red cell density fractions on a Stractan column having a discontinuous density gradient.

composition, were prepared by mixing fractions. Table II gives the results of the measurements made on these mixtures. Considering the variations of the four measured quantities over the nine different samples used in this experiment, it is apparent that the HC distribution width, σ_{HC}, is most sensitive to variations in the cellular composition of a blood sample, having a coefficient of variation of 39%. The next most sensitive quantity was σ_V with a coefficient of variation of 14%. The sensitivity of the measured HC distribution to the cellular composition of a blood sample is made very evident by the bimodal HC histogram and the cytogram from the mixture consisting of 50% F_1 and 50% F_2, Fig.

Table II. System Measurement Results for Samples Consisting of Various Mixtures of the Density-Separated Fractions Defined in Table I

Mixture	MCHC (g/dliter)	σ_{HC} (g/dliter)	MCV (fliter)	σ_V (fliter)
$\frac{1}{2}(F_1 + F_5)$	35.6	4.8	81.4	15.3
$\frac{1}{5}(F_1 + F_2 + F_3 + F_4 + F_5)$	34.9	3.6	83.2	12.9
$\frac{1}{4}F_1 + \frac{1}{2}F_3 + \frac{1}{4}F_5$	34.9	3.7	83.1	13.1
$\frac{1}{10}F_1 + \frac{4}{5}F_3 + \frac{1}{10}F_5$	34.4	2.7	83.9	11.6

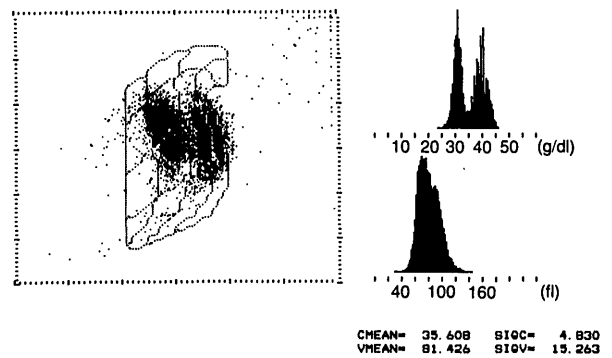

Fig. 15. Cytogram and histograms obtained from a blood sample prepared by mixing equal parts of the lowest and highest density fractions.

15. Collectively, the results of this experiment clearly demonstrate the unique ability of the present method to accurately and precisely measure the refractive index and, hence, the hemoglobin concentration of individual red blood cells.

While all the experiments described above were performed using a diode laser light source emitting radiation at $\lambda = 0.842\ \mu m$, the method has also been tested with He–Ne lasers emitting at either 0.6328 or 1.153 μm. The results obtained are in agreement with those presented here.

VI. Absolute Calibration

In the experimental tests described above, the gains G_1 and G_2 were set such that the average values of MCV and MCHC measured by the system on a small set of normal blood samples agreed with the averages of MCV and MCHC obtained using standard hematological reference methods. This calibration technique is generally acceptable in the clinical laboratory even though the two methods are measuring the properties of the cells in different cellular environments. A system calibration which uses particles whose volumes and refractive indices in the flow cell are accurately known is referred to as an absolute optical calibration.

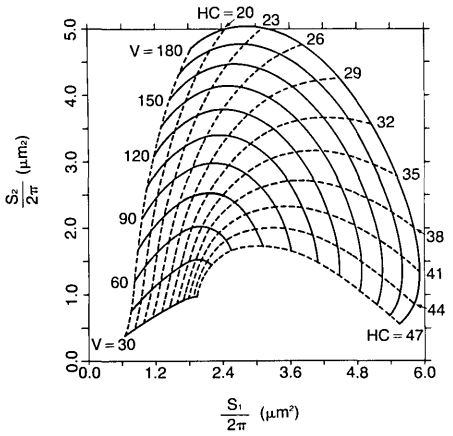

Fig. 16. The (S_1,S_2) to (V,HC) mapping for the optical system used to test the oil droplet calibration method. System parameters: $\lambda = 0.6328\ \mu m$, $n_s = 1.3339$, $n_0 = 1.345$, $\alpha = 0.001942$ dliter/g, $\epsilon_{\mu M} = 0.1616\ cm^2/\mu M$, $\theta_1 = 2.0°$, $\Delta\theta_1 = 1.0°$, $\theta_2 = 5.0°$, $\Delta\theta_2 = 10.0°$.

Commercially produced latex microspheres are available in the size range of red blood cells. However, latex materials have refractive indices in the neighborhood of 1.6 rather than 1.4, the typical value of n_R for red cells. Consequently, they cannot be used for absolute optical calibrations.

Ornstein[22] suggested that droplets of a water-immiscible oil suspended in the aqueous sheath fluid of the flow cell hydraulic system would be suitable calibration particles. A number of such oils, having refractive indices in the red cell range, are readily available. The refractive indices of these oils can be measured precisely using standard refractometers. Shaking a mixture of oil and sheath fluid produces a suspension of oil droplets having a wide range of sizes and a single, accurately known index of refraction. This suspension can be aspirated by the measurement system exactly as is done with sphered red cell samples. If the gains G_1 and G_2 are correctly set, the signal pairs (S_1,S_2) produced by the oil droplets will all fall on the constant-HC curve in the cytogram corresponding to the refractive index of the oil. The range of droplet sizes includes the full RBC volume range. Since the constant-HC contours are generally not linear and all values of V are included in the oil droplet sample, it is possible to calibrate without having made any independent volume measurements. Any ambiguity in the choices of G_1 and G_2 can be resolved by running calibrations using several oils having different refractive indices.

The above calibration procedure was tested using an optical system similar to that of Fig. 6 with a 2-mW linearly polarized He–Ne laser (Uniphase 1103P) as the light source. The high-angle and low-angle intervals were 5–15° and 2–3°, respectively. As can be seen in the (S_1,S_2) plot of Fig. 16, this choice of angle parameters yields a solvable system. The electronics system was similar to the one depicted in Fig. 8 but used a 2-D pulse height distribution of 50 × 50 channels instead of 64 × 64.

The $(S_1,S_2) \rightarrow (V,HC)$ mapping represented by Fig. 16 was computed with $\epsilon_{\mu M} = 0.1616\ cm^2/\mu M$ in Eq. (2),

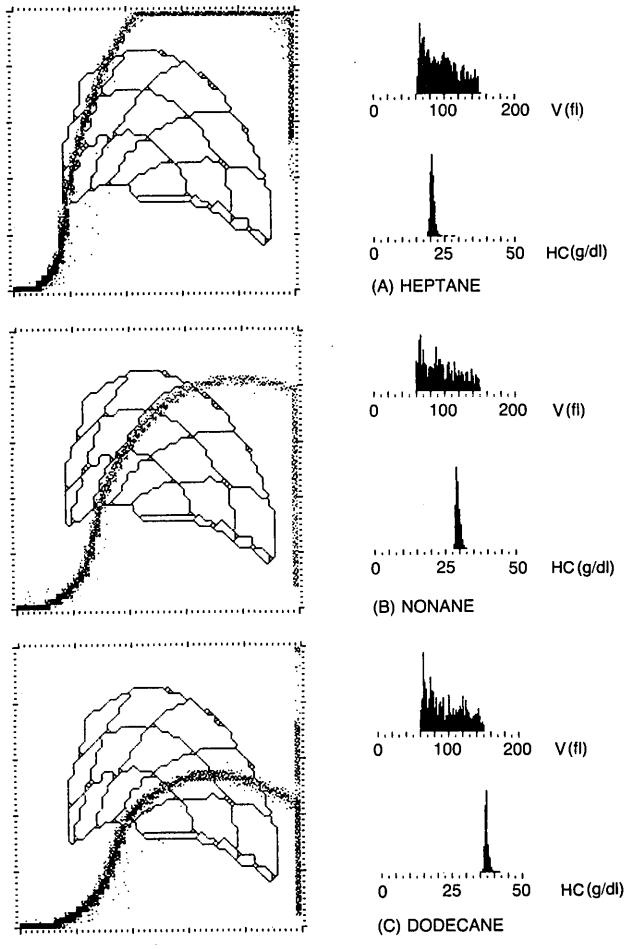

Fig. 17. Cytograms and histograms from measurements on oil droplet samples using the He–Ne laser system (Fig. 16).

whereas the calibration oils are nonabsorbing. Since the above value of $\epsilon_{\mu M}$ is, in fact, quite small (e.g., $n_I = 5 \times 10^{-5}$ when HC = 48 g/dliter), the error caused by using this mapping for oil droplet calibrations is entirely negligible relative to the electronic and digitization noise which was ~2% of the average signal.

Oil droplet measurements were made using three different oils: heptane, nonane, and dodecane. The purity of the oils was 99%. The refractive indices of the oils were measured with a Bausch & Lomb Abbe-3L refractometer adapted to accept a diffused He–Ne laser beam light source. Oil droplet samples were prepared by adding ten drops of an oil to 5 mliter of sheath fluid and shaking the mixture briskly for a few seconds. The cytograms and histograms obtained for the three oil droplet samples after optimizing the gains are shown in Fig. 17. In the analysis of these pulse height distributions, the $(S_1,S_2) \rightarrow (V,HC)$ mapping tables were restricted to volumes between 60 fliter and 150 fliter.

The data points in the cytograms fall in narrow bands which clearly follow the constant-HC (i.e., constant refractive index) contours. Consequently, the HC histograms are very narrow while the volume histograms are relatively flat over the range accepted for analysis. The quantitative results are given in Table III. Re-

Table III. Refractive Indices of the Oils Used in the Oil Droplet Samples and the Results of System Measurements on the Samples

Oil	Refractive index (at 0.6328 μm)	MCHC (g/dliter)	σ_{HC} (g/dliter)	n_R[a]
Heptane	1.3846	20.7	0.8	1.3852
Nonane	1.4022	29.4	0.7	1.4021
Dodecane	1.4184	37.4	0.7	1.4176

[a] The column labeled n_R gives the refractive indices derived from the measured MCHC values using the formula $n_R = 1.345 + 0.001942 \cdot \text{MCHC}$.

ferring to Eq. (1), the rms difference of 0.0006 between the n_R values and the refractometrically measured indices of refraction indicates that the accuracy of MCHC measurements made with this system is ±0.3 g/dliter or ~1%. The σ_{HC} results represent the instrumental limit on the precision of HDW measurements. A large part of this precision limit is due to the 2% signal digitization error associated with the 50 × 50 channel pulse height analysis. This is clear from the staircase quality of the cytogram data in Fig. 17.

VII. Conclusion

A new method has been described for simultaneously and independently determining the volume and hemoglobin concentration of individual sphered red blood cells from measurements of scattered monochromatic light at two carefully chosen angular intervals. This two-angle scattering methodology is based on the fact that, for certain pairs of angular intervals, Mie scattering theory may be used to compute one-to-one mappings between the two scattering cross sections (S_1,S_2) and the volume and hemoglobin concentration variables (V,HC). Although the present emphasis has been on the measurement of red cell properties, in principle the method has more general applicability. Specifically, it applies to spherical particles that are either (i) nonabsorbing or (ii) have real and imaginary parts of the refractive index which depend in a known way on a single intensive property of the particles. Red blood cells are an example of the latter case; n_R and n_I are related to the intensive property HC through Eqs. (1) and (2).

Flow-cytometric experiments confirmed the ability of the new method to measure the clinically relevant red cell parameters MCV and MCHC. The results of these experiments agree closely with measurements made using standard reference methods. Statistically, comparisons show that the experimentally determined MCV and MCHC values are at least as accurate and precise as those produced by reference methods. Furthermore, the results prove that the new method eliminates the problem of MCHC interference with MCV measurements which has limited the accuracy of the current generation of automated hematology instruments. In addition, the feasibility of measuring the frequency distribution of cell hemoglobin concentration has been demonstrated.

The two-angle scattering methodology can produce absolute measurements of particle volume and refractive index if a suitable calibration sample is available. Experiments with samples prepared as suspensions of water-immiscible oil droplets yielded refractive-index measurements which agreed with known values to the precision limit set by the digital signal processing. Therefore, the techniques employed in these oil droplet experiments constitute an absolute optical calibration procedure for the new method.

We wish to thank Narla Mohandas of the University of California, San Francisco, for preparing the density-separated samples and the samples with altered hydration states. Our thanks to Y. R. Kim who provided us with the RBC sphering reagents. We greatly appreciate the excellent engineering support provided by J. Orlik and the valuable contributions of G. M. Colella and D. Burger to the experiments. Many fruitful discussions with Leonard Ornstein of the Mt. Sinai School of Medicine influenced the course of our work. We are indebted to W. Groner, who initiated this project, for providing us with the necessary resources and for his encouragement.

References

1. For concise reviews of the subject and extensive bibliographies, see T. M. Jovin *et al.*, "Automatic Sizing and Separation of Particles by Ratios of Light Scattering Intensities," J. Histochem. Cytochem. **24**, 269 (1976); G. C. Salzman, "Flow Cytometry: The Use of Lasers for Rapid Analysis and Separation of Single Biological Cells," in *The Biomedical Laser*, L. Goldman, Ed. (Springer, New York, 1981), Chap. 5.
2. L. P. Bayvel and A. R. Jones, *Electromagnetic Scattering and Its Applications* (Applied Science, London, 1981), pp. 22–47.
3. M. M. Wintrobe *et al.*, *Clinical Hematology* (Lea & Febiger, Philadelphia, 1981), p. 18.
4. J. D. Bessman and R. K. Johnson, "Erythrocyte Volume Distribution in Normal and Abnormal Subjects," Blood **46**, 369 (1975).
5. H. E. Kubitschek, "Electronic Measurement of Particle Size," Res. Appl. Ind. **13**, 128 (1960.
6. N. Mohandas *et al.*, "Inaccuracies Associated with the Automated Measurement of MCHC in Dehydrated Cells," Blood **56**, 125 (1980).
7. T. Arnfred, S. D. Kristensen, and V. Munck, "Colter Counter Model S and Model S-Plus Measurements of Mean Erythrocyte Volume (MCV) are Influenced by the Mean Erythrocyte Haemoglobin Concentration (MCHC)," Scand. J. Clin. Lab. Invest. **41**, 717 (1981).
8. Y. R. Kim and L. Ornstein, "Isovolumetric Sphering of Erythrocyte for More Accurate and Precise Cell Volume Measurement by Flow Cytometry," Cytometry **3**, 419 (1983).
9. M. Kerker, *The Scattering of Light and Other Electromagnetic Radiation* (Academic, New York, 1969), Chap. 3.
10. Ref. 3, Chap. 4.
11. R. Barer and S. Joseph, "Refractometry of Living Cells," Q. J. Microsc. Sci. **95**, 399 (1954).
12. Ref. 9, chap. 8.
13. R. B. Pennell, "Composition of Normal Human Red Cells," in *The Red Blood Cell*, C. Bishop and D. M. Surgenor, Eds. (Academic, New York, 1964), Chap. 2.
14. R. S. Longhurst, *Geometrical and Physical Optics* (Longman, London, 1967), pp. 446–448.
15. O. W. van Assendelft, *Spectrophotometry of Haemoglobin Derivatives* (van Gorcum, Assen, The Netherlands, 1970, pp. 23–25 and Chap. 3.

and Chap. 3.
16. H. P. Mansberg, A. M. Saunders, and W. Groner, "The Hemalog D White Cell Differential System," J. Histochem. Cytochem. **22,** 711 (1974).
17. National Committee for Clinical Laboratory Standards (NCCLS), Publication H7-T (1981).
18. International Committee for Standardization in Haematology, J. Clin. Pathol. **31,** 139 (1978).
19. M. R. Clark *et al.*, "Study on the Dehydrating Effect of the Red Cell Na^+/K^+-Pump in Nystatin-Treated Cells with Varying Na^+ and Water Contents," Biochim. Biophys. Acta **646,** 422 (1981).
20. L. M. Corash *et al.*, "Separation of Erythrocytes According to Age on a Simplified Density Gradient," J. Lab. Clin. Med. **84,** 147 (1974).
21. M. R. Clark, A. C. Greenquist, and S. B. Shohet, "Stabilization of the Shape of Sickled Cells by Calcium and A23187," Blood **48,** 899 (1976).
22. L. Ornstein, Mt. Sinai School of Medicine; private communication.

Meetings Calendar *continued from page 1354*

1985

December

8–13 10th Ann. Int. Conf. on Infrared & Millimeter Waves, Lake Buena Vista, Fla. *K. Button, MIT Natl. Magnet Lab., Bldg. NW14, Cambridge, Mass. 02139*

1986

? 3rd Int. Conf. on Metal-Organic Vapor Phase Epitaxy, Pasadena *N. Bottka, Naval Res. Lab., Electronic Material Tech. Branch, Wash., D.C. 20375*

January

19–24 Optical & Electro-Optical Eng. Symp., Los Angeles *SPIE, P.O. Box 10, Bellingham, Wash. 98227*

February

9–15 Astronomical Instrumentation Conf., Tucson *SPIE, P.O. Box 10, Bellingham, Wash. 98227*

13–14 **Optical Fiber Sensors, OSA Top. Mtg.,** San Diego *OSA Mtgs. Dept., 1816 Jefferson Pl., N.W., Wash., D.C. 20036*

24–26 Optical Fiber Communication Conf., Atlanta *OSA Mtgs. Dept., 1816 Jefferson Pl., N.W., Wash., D.C. 20036*

26–28 Integrated & Guided-Wave Optics Top. Mtg., Atlanta *OSA Mtgs. Dept., 1816 Jefferson Pl., N.W., Wash., D.C. 20036*

March

9–14 Microlithography Conf., Santa Clara *SPIE, P.O. Box 10, Bellingham, Wash. 98227*

31–4 Apr. Optics & Electro-Optics, 1986 Tech. Symp. East, Arlington *SPIE, P.O. Box 10, Bellingham, Wash. 98227*

April

13–23 3rd Int. Conf. on Optical & Electro-Optical Applied Science & Engineering, Innsbruck *SPIE, P.O. Box 10, Bellingham, Wash. 98227*

22–26 Laser Safety: Hazard, Inspection & Control course, Chicago *Laser Inst. of Amer., M. McHenry, 5151 Monroe St., Suite 118W, Toledo, Oh. 43623*

June

2–6 Optical & Electro-Optical Engineering Symp., Quebec *SPIE, P.O. Box 10, Bellingham, Wash. 98227*

9–13 Quantum Electronics Int. Conf., San Francisco *OSA Mtgs. Dept., 1816 Jefferson Pl., N.W., Wash., D.C. 20036*

10–13 **Conf. on Lasers & Electro-Optics (CLEO '86),** San Francisco *OSA Mtgs. Dept., 1816 Jefferson Pl., N.W., Wash., D.C. 20036*

16–19 **Ultrafast Phenomena, OSA Top. Mtg.,** Snowmass, Colo. *OSA Mtg. Dept., 1816 Jefferson Pl., N.W., Wash., D.C. 20036*

July

7–11 Optical Computing Int. Conf., Jerusalem *ICO, P.O. Box 4413, 61044 Tel-Aviv, Israel*

16–18 Image Detection & Quality Int. Top. Mtg., Paris *P. Chavel, Institut d'Optique, B.P. 43, 91406 Orsay-Cedex, France*

August

17–22 30th Ann. Int. Symp. on Optical & Electro-Optical Eng., San Diego *SPIE, P.O. Box 10, Bellingham, Wash. 98227*

14–19 Optical & Electro-Optical Engineering Symp., Cambridge *SPIE, P.O. Box 10, Bellingham, Wash. 98227*

September

14–19 Optical & Electro-Optical Eng. Symp., Cambridge *SPIE, P.O. Box 10, Bellingham, Wash. 98227*

October

5–10 Optical & Electro-Optical Eng. Symp., Cambridge *SPIE, P.O. Box 10, Bellingham, Wash. 98227*

21–24 **OSA Ann. Mtg.,** Los Angeles *OSA Mtgs. Dept., 1816 Jefferson Pl., N.W., Wash., D.C. 20036*

November

10–13 5th Int. Congr. on Applications of Lasers & Electro-Optics, Boston *H. Lee, Laser Inst. of Am., 5151 Monroe St., Suite 118W, Toledo, Ohio 43623*